

Modelling and parameters for mineral-aqueous reaction kinetics

(devPhase project)

by KD44, TB44 draft 9 Feb 2, 2015

1. Introduction: Methods of GEM simulations of mineral-aqueous reaction kinetics

Aquatic chemical systems at Earth surface conditions rarely achieve the truly reversible equilibrium state. No mineral solid precipitates or dissolves instantly; at room temperature T and pressure P , some coarse-crystalline phases are almost unreactive; others (e.g. clays) dissolve relatively fast, but do not precipitate. Particulate solid nanophases with large specific surface areas are metastable with respect to their bulk counterparts due to the positive surface free energy contribution (Wu and Nancollas, 1999; Navrotsky, 2011). Hence, the phase metastability and solid-aqueous reaction kinetics must be accounted for in any realistic chemical thermodynamic model of a complex aquatic system. This becomes critical when chemical thermodynamic models are embedded in reactive transport simulations, performed using the coupled codes such as PHAST (Parkhurst et al., 2010) or OpenGeoSys-GEM (Shao et al., 2009) that combine a fluid transport model with the chemical speciation solver, using a discretization of the system in space (many small enough control volumes) and in time (many small enough time steps Δt). In such simulations, based on the *principles of local and partial equilibrium*, the missing or incorrect account for mineral-aqueous reaction kinetics usually leads to intractably small time steps and/or to completely unrealistic predictions.

1.1. Local and partial equilibrium

The *local equilibrium* is assumed to take place in each control volume, according to the assigned composition and the thermodynamic parameters of state (P, T , surface areas of phases A). The *partial equilibrium* occurs if some components in some phases cannot reach their equilibrium amounts because of the *additional metastability restrictions* (AMR). All phases and components without AMR take part in the achievement of the partial equilibrium state under the mass balance common to the whole system.

Thus, a chemical speciation solver that can handle AMRs, such as the GEM-Selektor (Karpov et al., 2001; Kulik et al., 2013; Wagner et al., 2012), can be directly employed for simulating the kinetics of a time-dependent chemical process by setting each AMR as a function of the time step duration Δt , the time variable t , the surface area $A_{k,t}$ of k -th solid phase, and the (absolute) net kinetic rate $R_{n,k,t}$ (details are given below). In principle, AMRs may also depend on a link of the specific surface or kinetic rates for one phase (e.g. an overgrowth, adsorbed layer) to the volume or surface area of another, “seed”, “substrate” or “adsorbent” phase, which may even be inert, or may have its own kinetics.

In a stepwise simulation, the mole amount $n_{k,t+\Delta t}$ of the solid at time $t+\Delta t$ is set by the upper AMR

$\bar{n}_{k,t+\Delta t}$ for precipitation or by the lower AMR $\underline{n}_{k,t+\Delta t}$ for dissolution:

$$\begin{aligned}\bar{n}_{k,t+\Delta t} &= n_{k,t} + A_{k,t} R_{k,t} \Delta t && \text{if } \log_{10} \Omega_k > \varepsilon \\ \underline{n}_{k,t+\Delta t} &= n_{k,t} - A_{k,t} R_{k,t} \Delta t && \text{if } \log_{10} \Omega_k < -\varepsilon\end{aligned}\quad (1.1),$$

where $0 < \varepsilon < 10^{-5}$ is a numerical tolerance. The direction of change depends on the sign of the logarithmic phase stability index $\log_{10} \Omega_k$ (explained below). The surface area of the k -th solid phase is obtained as $A_{k,t} = A_{S,k} M_{M,k} n_{k,t}$, where $A_{S,k}$ is the specific surface area ($\text{m}^2 \text{kg}^{-1}$); $M_{M,k}$ is the molar mass (kg mol^{-1}), and $n_{k,t}$ is the current amount (mol) of the k -th phase.

The implementation of metastability and kinetics differs from code to code; so far, there is no conventional data structure for kinetic parameters. Large literature exists on experimental data and kinetic rate laws and parameters of mineral-aqueous reactions (e.g. Teng et al., 2000; Schott et al., 2009, 2012), with a much higher degree of understanding of dissolution compared to that for precipitation and nucleation. Because the experimental rate constants are typically normalized per unit area, they must be scaled by the current reactive surface area of the mineral, which depends on many factors, some of them are external to the chemical system, and some related to the particle/pore morphology, initial size distributions, and surface roughness. At present, this is perhaps the most important knowledge gap in geochemistry of the mineral – water interfaces (Marini et al., 2000; Mironenko and Zolotov, 2012; Scislewski and Zuddas, 2010), related in reactive transport modeling to the impact of porosity changes on transport parameters and on reactive surface areas. Many kinetic rate laws contain the activity product term related to a particular reaction mechanism, catalysis, inhibition, etc. (Schott et al., 2012; Palandri and Kharaka, 2004). Near-equilibrium kinetic rates also depend on the *affinity term* based on the *phase saturation index* Ω_k ; particular forms of this term reflect different nucleation, growth or dissolution mechanisms.

1.2. Gibbs energy minimization (GEM) method

The GEM IPM algorithm (Kulik et al., 2013), as implemented in the in-house GEM software, has a great potential for thermodynamic modeling of mineral-water reaction kinetics with multiple reaction pathways because it can directly handle metastability restrictions. In GEM IPM, the chemical system is defined by a bulk composition vector, $n^{(b)}$, specifying the input amounts of chemical elements and charge; the standard molar Gibbs energies of all dependent components (species), g° , at T, P of interest; the parameters of (non)ideal models of mixing in solution phases (Wagner et al., 2012), needed to calculate activity coefficients λ_j of species indexed with j ; and the optional AMRs. After each run, the GEM *primal* (speciation vector $\hat{n}^{(x)}$) and the *dual* (vector $\hat{u}^{(b)}$) of chemical potentials of chemical elements and charge results provide concentrations and activities of all aqueous species, as well as activities and amounts of all components in each phase. The stability index Ω_k of any phase, even of that absent from the mass balance, is found as a *dual-thermodynamic* estimate of the sum of (anticipated) mole fractions \hat{x}_j of all phase components:

$$\Omega_k = \sum_j \hat{x}_j = \sum_j \exp\left(\hat{\eta}_j - \frac{g_j^o}{RT} - \ln \lambda_j - \Xi_k\right) \quad (1.2)$$

where the index j runs over all components in the phase; R is the universal gas constant; Ξ_k is a term for converting species concentration into the common mole fraction scale (e.g. $\ln P$ for gases; $\ln 55.5085$ for aqueous species); and $\hat{\eta}_j$ stands for the *dual-solution chemical potential*

$$\hat{\eta}_j = \sum_i a_{ij} \hat{u}_i^{(b)} \quad (1.3)$$

where index i runs over all chemical elements and charge, and a_{ij} is the formula stoichiometry coefficient of i -th element in j -th species (e.g. 2 for O in SiO_2).

In the GEM IPM algorithm, the Ω_k index (eq 1.2) is used as the *criterion of stability* for any phase. If, numerically, $-0.01 < \log_{10}\Omega_k < 0.01$ then the positive or zero amount of this phase is in equilibrium with the rest of the system. If $\log_{10}\Omega_k < -0.01$ then the phase is unstable (under-saturated), but may be kept in a positive amount in the mass balance by the lower AMR(s) \underline{n}_j set on some or all of its components. If $\log_{10}\Omega_k > 0.01$ then the phase is over-stable (oversaturated) because the positive or zero upper AMR(s) \bar{n}_j were set on some of its components from above.

Taken together, the GEM output phase stability index Ω_k together with the input lower- \underline{n}_j and upper \bar{n}_j AMRs make the GEM-Selektor code a versatile tool for modelling various kinds of kinetics and metastability, represented as sequences of partial (restricted) equilibrium states. Thus, lower-AMRs allow stepwise simulation of *dissolution* of a mineral as long as its stability index $\Omega_k < 1$; upper-AMRs allow stepwise simulation of mineral *precipitation* as long as $\Omega_k > 1$. Setting AMRs as a function of time according to the chosen kinetic rate law allows the GEM software to simulate the kinetics of mineral-aqueous reactions and trace element uptake. The more ample information about the mineral-aqueous reaction is available from the experiment the more accurate and specific form of the rate equation can be applied to the system of interest.

2. The TKinMet library of models of mineral-aqueous reaction kinetics

Some kinetic rate equations for dissolution, precipitation, and trace element uptake in solid solutions have been implemented in the TKinMet code library used in GEM-Selektor and GEMS3K codes. Eventually, with this library, GEMS will become a general and flexible software tool, extending and superseding the existing (geo)chemical models and codes capable of kinetic simulations (Parkhurst and Appelo 1999; Made et al., 1994; Fritz et al., 2009; Mironenko and Zolotov, 2012). In the TKinMet library, mineral-water interaction kinetic rate laws are considered in a general form derived from (Lasaga, 1998; Palandri and Kharaka, 2004; Schott et al., 2012):

2.1. Theoretical background and kinetic rate parameters

Most mineral-aqueous (mineral-gas) kinetic rate equations can be expressed using a general form (after [Schott et al., 2012]), written here with GEM notation indices as:

$$\frac{dn_k}{dt} = -A_k \sum_r^{n(r)_k} \left\{ \theta_{k,r} \cdot \left(\kappa_{k,r}^o \Lambda_{k,r} e^{\frac{-E_{k,r}}{RT}} \right) \cdot f(\Pi a)_{k,r} \cdot f(\Omega)_{k,r} \right\} = R_p A_k \quad (2.1)$$

where $k \in \Phi$ is the index of (solid) phase;

n_k is the mole amount of k -th phase at time t ;

A_k is the current surface area (or pore volume) of k -th phase in m^2 (or m^3) – time-dependent, may either depend on a built-in model of particle size/area evolution or be externally controlled e.g. from the mass transport code;

R_p is the total net growth (or dissolution) rate (in $\text{mol}/\text{m}^2/\text{s}$);

$n(r)_k$ is the number of «parallel reactions» that affect the amount of k -th phase (1, 2, 3, ...), 1 by default;

r is the index of one of these «reactions» (0 by default), called “xPR” in the program; dissolution, nucleation, and precipitation should be treated as different parallel reactions;

$\theta_{k,r}$ is the effective fraction of k -th phase surface area (or pore volume) that corresponds to the effective area (pore volume) where the r -th «reaction» occurs (1 by default) – time-dependent, externally controlled e.g. from the mass transport code.

$\left(\kappa_{k,r}^o \Lambda_{k,r} e^{\frac{-E_{k,r}}{RT}} \right)$ is the «reaction» rate constant term including temperature correction, where:

$\kappa_{k,r}^o$ is the rate constant at reference temperature in $\text{mol m}^{-2}\text{s}^{-1}$ (or $\text{mol m}^{-3}\text{s}^{-1}$) or other appropriate units;

the sign convention of $\kappa_{k,r}^o$ is: positive sign for dissolution and negative for precipitation; T is temperature in K;

$\Lambda_{k,r}$ is the Arrhenius parameter (1 by default); R is the universal gas constant ($8.31451 \text{ J K}^{-1} \text{ mol}^{-1}$);

$E_{k,r}$ is the activation energy (J mol^{-1}) of r-th «parallel reaction» involving k -th solid phase; the expression

$e^{\frac{-E_{k,r}}{RT}}$ is sometimes represented in a different form: $e^{\frac{-E_{k,r}^*}{R} \left(\frac{1}{T} - \frac{1}{298.15} \right)}$; both forms are connected through a

$$\text{relation: } \Lambda_{k,r} \cdot e^{\frac{-E_{k,r}}{RT}} = \Lambda_{k,r}^* \cdot e^{\frac{-E_{k,r}^*}{R} \left(\frac{1}{T} - \frac{1}{298.15} \right)}$$

So, to use Palandri's terms [Palandri & Kharaka, 2004] within the general equation, we need to input

$$\Lambda_{k,r} = \Lambda_{k,r}^* \cdot e^{\frac{E_{k,r}^*}{R \cdot 298.15}}$$

where $\Lambda_{k,r}^*$ is the Arrhenius parameter coming from Palandri's report. We assume that $E_{k,r}^* = E_{k,r}$.

$$f(\Pi a)_{k,r} = I^{b_{I,k,r}} \text{pH}^{b_{\text{pH},k,r}} \text{pe}^{b_{\text{pe},k,r}} \text{Eh}^{b_{\text{Eh},k,r}} \left(\prod_j^{n(j)_{k,r}} a_{j,k,r}^{b_{j,k,r}} \right)^{p_{k,r}} \quad (2.2)$$

is the activity product term (sometimes called «reaction catalysis» term), where:

I is the (effective molal) ionic strength, and $b_{I,k,r}$ is the empirical parameter related to I (default 0); $b_{\text{pH},k,r}$ is the empirical parameter related to pH (default 0); $b_{\text{pe},k,r}$ is the parameter related to pe (default 0); $b_{\text{Eh},k,r}$ is the parameter related to Eh, V (default 0);

$p_{k,r}$ is the «reaction order» parameter for the far-from-equilibrium case (default 1);

$n(j)_{k,r}$ is the number of (aqueous or gaseous or surface) species from other reacting phases involved;

$a_{j,k,r}$ is the activity (fugacity) of j -th species ($a_{\text{H}^+} = 10^{-\text{pH}}$, $a_e = 10^{-\text{pe}}$);

$b_{j,k,r}$ is the (reaction stoichiometry coefficient) parameter (default 0).

$f(\Omega)_{k,r}$ in eq (2.1) is the affinity term for r -th reaction involving this k -th solid phase, which can take several different forms, all using the current k -th phase stability (saturation) index Ω_k computed in GEM IPM (see GEMS3K paper Kulik ea 2013, eq B-10). The different forms of affinity term used in «parallel reaction» contributions reflect different growth or dissolution mechanisms; these forms are selected using the $\text{oCPR}(k, r)$ integer flag, with values indicated below in brackets, e.g. (0) – default term.

$$(0) (u_{k,r} + 1 - \Omega_k^{q_{k,r}})^{m_{k,r}}$$

$$(1) (\Omega_k^{q_{k,r}} - 1 - u_{k,r})^{m_{k,r}}$$

In «classic» transitional states theory (0) and (1) forms, $q_{k,r}$ and $m_{k,r}$ are the reaction order parameters (default values = 1 and 0, respectively). The $u_{k,r}$ is the empirical parameter augmenting the constant in the affinity term (default value is 0, may be equal to 1 or ...).

(2) $e^{-u_{k,r}/\Omega_k}$ [Schott et al. 2012 Fig. 1e] where $u_{k,r}$ is the empirical parameter (default value 0).

(3) $1 - e^{-(q_{k,r} \ln \Omega_k)^{u_{k,r}}}$ [Hellmann & Tisserand, 2006 eq (9)], where $q_{k,r}$ and $u_{k,r}$ are the reaction order parameters (default values = 1).

(4) $u_{k,r} (\Omega_k - 1) \cdot \ln \Omega_k$ [Teng et al., 2000, eq (13)] where $u_{k,r}$ is the empirical parameter (default 1).

(5) $\Omega_k^{m_{k,r}}$ [Teng et al., 2000, Fig. 6] where $m_{k,r}$ is the empirical parameter (default 0).

(6) $(\Omega_k - \Omega_{k,\text{eff}})^{m_{k,r}}$ for nucleation and growth, where $\Omega_{k,\text{eff}}$ is the «effective» saturation index (an input empirical parameter related to the mineral), and $m_{k,r}$ is the empirical parameter (default 0).

(7) Hellevang (Pham et al., 2011; Hellevang et al., 2013) CNT nucleation rate equation (2.4).

Hellevang et al. (2013, 2011) suggested a simplified equation for nucleation rate based on CNT (see Pham et al., 2011, eqs 3,4). The CNT (classical nucleation theory) equation (e.g. Nielsen, 1983) defines the nucleation rate J (in nuclei per second per kg H₂O (or per dm³ H₂O in dilute electrolyte)) as

$$J = k_N \exp \left\{ -\beta N_A f(\theta) \left(\frac{\nu \sigma^{3/2}}{(RT)^{3/2} \ln \Omega} \right)^2 \right\} \quad (2.3)$$

where k_N is the nucleation rate constant; β is the geometric shape factor; $f(\theta)$ is the correction factor for heterogeneous nucleation, ν is the molar volume, and σ is the specific surface energy (surface tension).

CNT shows that no nuclei form at very low supersaturation, and fewer and larger nuclei form at low temperature and low supersaturation. Eq (2.3) was simplified by Pham et al. 2011 to

$$r_N = k_N \exp \left\{ -\Gamma \left(\frac{1}{T^{3/2} \ln \Omega} \right)^2 \right\} \quad (2.4)$$

where parameter Γ contains all parameters from the above CNT equation except T and Ω , and the nucleation rate constant is expressed in units of mol/(kgH₂O)/s. Its value for Ca,Mg carbonates was roughly estimated by Pham et al. to be $k_N \approx 1$ mol/(kgH₂O)/s (can range +/- 10 orders of magnitude), with $\Gamma = (4 \pm 1) \cdot 10^{10}$ K³ consistent to that value of k_N (Pham et al. 2011).

Parameters (for dolomite): $k_N = 1$ mol/(kgH₂O)/s $\Gamma = (4 \pm 1) \cdot 10^{10}$ K³

In eq. (2.1), $dn/dt/A$ is taken in mol/m²/s, as default units. The linear growth velocity (or radial velocity for large enough spherical particles) will then be in m/s units. It is related to molar growth rate as

$$R_{L,k} = 3 \cdot 10^9 \frac{M_k}{\rho_k} R_p \quad (2.5)$$

where $R_{L,k}$ is the net average linear growth (or dissolution) velocity in nm/s, $R_p = \frac{1}{A_k} \frac{dn_k}{dt}$ is the net

growth (or dissolution) rate, M_k is the molar mass of the phase in g/mol, ρ_k is the mineral density in g/m³. Because $M_k/\rho_k = 10^{-6} V_{M,k}$ where $V_{M,k}$ is the mineral molar volume in cm³/mol, this equation also can be written as $R_{L,k} = 3 \cdot 10^3 V_{M,k} R_p$.

2.2. Equations and parameters for the surface area correction upon growth or dissolution

Specific surface area of the mineral is defined as $A_{S,k} = A_k / m_k$ (in m²·kg⁻¹) or $A_{V,k} = A_k / V_k$ (in m⁻¹).

Upon growth or dissolution, both $A_{S,k}$ and $A_{V,k}$ values vary with time because of changing particle size, shape, and surface roughness. Hence, in kinetic simulations, specific surface areas must be corrected after each time step, either internally in TKinMet library functions, or externally controlled by the reactive transport model.

In the simplest case, for homogeneous-size particles:

$$A_{S,k} = \Psi_k \cdot A_{S,k,0} \left(\frac{n_k}{n_{k,0}} \right)^{-\frac{1}{3}} \quad (2.6)$$

where $A_{S,k}$ is the current surface area of k-th phase in m², $A_{S,k,0}$ is the initial surface area, Ψ_k is the shape factor (default value=1 for spherical particles), n_k is the current mineral mole amount, $n_{k,0}$ is the initial mole amount. The power coefficient is negative for precipitation (as shown in eq 1.4) and positive for dissolution, in which case the specific surface area increases when n_k decreases.

In the more general case, currently implemented in the TKinMet library, for particles of uniform size and shape, and assuming no density change of the mineral upon growth and no other second-order effects,

$$A_{V,k,t} = A_{V,k,t-\Delta t} \frac{\psi_{k,t-\Delta t}}{\psi_{k,t}} \frac{d_{VS,k,t-\Delta t}}{d_{VS,k,t} + 2R_{L,k,t}\Delta t} \quad (2.7)$$

where $A_{V,k,t}$ is the initial specific surface area; $d_{VS,k}$ is the mean particle volume-surface diameter; and $R_{L,k}$ is the current linear rate from eq (2.5). As the shape factor, we use the *sphericity* coefficient $0 < \psi_k \leq 1$ (Wadell, 1935), defined as:

$$\psi_k = \pi^{\frac{1}{3}} \frac{(6V_p)^{\frac{2}{3}}}{A_p} = \frac{6V_p}{d_p A_p} \quad (2.8)$$

where $d_p = d_{VS,k} = \sqrt[3]{\psi_k A_{V,k}}$ is the *estimated particle size*; $V_p = \frac{1}{6}\pi d_p^3$ is the *mean particle volume*; and $A_p = A_k \sqrt{\frac{V_p}{V_k}}$ is the *mean particle surface area*. Sphericity (eq 2.8) is the external parameter of the kinetics model; the initial ψ_o value must be defined together with other initial parameters at the beginning of simulations. From simple geometric considerations, perfect mineral crystals must have sphericity about 0.8 ± 0.1 ; values below 0.7 apply to thin platelets or to rough surfaces of aggregate particles.

In eq (2.7), the time evolution of sphericity describes the impact of changing morphology and surface roughness on the variation of specific surface area and thus onto dissolution or precipitation rates of the solid. Again, this evolution can be controlled externally (from the mass transport model), or represented as a function of some system parameters, for instance

$$\psi_k(t) = \psi_{0,k} + \psi_{1,k}u + \psi_{2,k}u^2 + \dots \quad (2.9)$$

where $\psi_{0,k}$, $\psi_{1,k}$, $\psi_{2,k}$, ... are the empirical coefficients, and the u variable can be e.g. the phase stability index $u = \log_{10} \Omega_{k,t}$, the relative change of phase amount $u = (n_{k,t} - n_{k,0})/n_{k,0}$, the function of growth rate $R_{L,k,t}$, of temperature T , or of other system variables.

At the same stoichiometry and chemical potential, the activity of any j -th component and the stability index of the whole phase Ω_k will depend on the value(s) of its standard-state per-mole Gibbs energy g_j^0 . In fact, the g_j^0 parameter can also reflect the differences in stability for polymorphic modifications of the same compound (e.g. amorphous calcium carbonate, vaterite, aragonite, calcite), as well as the impact of surface free energy (or interface tension) γ , or other energy factors. Therefore, we consider the g_j^0 term with its possible modifications and extensions as a main spot to connect thermodynamic models, kinetic rates, and crystallization pathways, in addition to the $\psi_{k,t} = f(t, n, \Omega, \dots)$ function and $\theta_{k,r,t}$ parameters for parallel reactions.

In the TKinMet library, some parameters, e.g. the dissolution rate constant, the activation energy, the reaction type and order constants for parallel reactions, are considered as chemical properties of the solid phase, kept in the respective phase definition record in GEMS project database. Other parameters, such as the shape factor function $\psi_{k,t} = f(t, n, \Omega, \dots)$ and reactive fraction $\theta_{k,r}$ of surface area assigned to r-th parallel reaction, are related to evolving particle or pore size and shape distributions. Such parameters may be set externally, e.g. on the basis of assumptions of the reactive-transport or the crystallization pathway model. These parameters with their variation should generally come into TKinMet calculations from the transport part of the coupled reactive transport code.

2.3. Aqueous - solid solution systems

For solid solutions, in the next partial equilibrium state at time $t+\Delta t$, the TKinMet codes will split the new AMR for the total amount of phase $\underline{n}_{k,t+\Delta t}$ into AMRs to the end members $\underline{n}_{j,t+\Delta t}^{(x)}$ (the symbols here refer to both upper- and lower cases in eqs (1.1)). There are several ways of such splitting, depending on a particular dissolution, precipitation, or nucleation process (this part of TKinMet code still under development). For example, the dissolution of a sparingly-soluble solid solution usually occurs stoichiometrically (Glynn and Reardon, 1990), which can be represented by changing AMRs for end members proportional to their mole fractions:

$$\begin{aligned}\underline{n}_{k,t+\Delta t} &= \underline{n}_{k,t} - A_{k,t} R_{k,t} \Delta t \quad \text{if } \log_{10} \Omega_k < -\varepsilon \\ \underline{n}_{j,t+\Delta t}^{(x)} &= \underline{n}_{j,t}^{(x)} + x_{j,t} (\underline{n}_{k,t+\Delta t} - \underline{n}_{k,t})\end{aligned}\tag{2.10}$$

Here, $x_{j,t}$ is the current mole fraction of j-th end member at time t , and the index j runs over all end members in the solid solution phase. The impact of another (secondary) phase precipitation on the dissolution rate $R_{n,k,t}$ is accounted for by changes in the saturation index $\Omega_{k,t}$ or explicitly by augmenting the shape factor $\psi_{k,t}$ or the reactive area fractions $\theta_{k,r}$. For nucleation and growth, such relationships become complex e.g. (Prieto, 2009) because such processes depend on the contribution of surface free energies that, in turn, depends on particle size and curvature.

In the present contribution, the case of uptake of a trace element (Tr) into a binary solid solution with the host element (Hc) is presented, as this case was foreseen in the SKIN project. Here, the rate law for the host mineral is applied to the whole solid solution phase, and used as the basis for the uptake kinetics model discussed in (Thien et al., 2014).

The distribution of a trace element Tr between the aqueous solution and the condensed crystalline solid (solution) relative to the host component Hc is usually described by the fractionation coefficient $\Delta_{Tr,Hc}$, which is the ratio of two distribution ratios R_d :

$$\Delta_{Tr,Hc} = \frac{R_d(Tr)}{R_d(Hc)} \quad (2.11)$$

The distribution ratio is defined as the ratio of component concentration in the solid to that in the aqueous phase. Taking mole fraction x for the solid and total dissolved molality [] for the aqueous part, equation (2.10) can be rewritten as follows:

$$\Delta_{Tr,Hc} = \left(\frac{x_{Tr}}{[Tr]} \right) / \left(\frac{x_{Hc}}{[Hc]} \right) \quad \text{or} \quad \Delta_{Tr,Hc} = \frac{x_{Tr}}{x_{Hc}} \cdot \frac{[Hc]}{[Tr]} \quad (2.12)$$

From the known fractionation coefficient $\Delta_{Tr,Hc}$ and the mole fraction x_{Hc} of Hc end member (usually unity or close to a constant if there are 2 or more host (major) end members), the mole fraction of Tr end member can be estimated as e.g.

$$x_{Tr} = \Delta_{Tr,Hc} x_{Hc} \frac{[Tr]}{[Hc]} \quad (2.13)$$

At every time step, the correction of upper and lower metastability constraints for the host Hc and trace Tr end members is done using the previous amount $n^{(x)}$ of the respective end member and an increment, which is calculated according to kinetic rates, Hc mole fraction, and the Tr mole fraction obtained from the corrected (eq 2.12) Tr fractionation coefficient:

$$\bar{n}_{Hc,t+\Delta t}^{(x)} = n_{Hc,t}^{(x)} + A_{k,t} R_{k,t} \Delta t \cdot x_{Hc,t} \quad (2.14)$$

$$\bar{n}_{Tr,t+\Delta t}^{(x)} = n_{Tr,t}^{(x)} + A_{k,t} R_{k,t} \Delta t \cdot x_{Tr,t} \quad \text{where } x_{Tr,t} = \Delta_{Tr,Hc,t} \frac{[Tr]_t}{[Hc]_t} \quad \text{and } x_{Hc,t} = 1 - x_{Tr,t} \quad (2.15)$$

Equations as (2.12) and (2.13) apply to several Hc and Tr end members in the solid solution phase, if x_{Hc} and $[Hc]$ in eqs (2.11 to 2.13) and (2.14) are re-defined as the sums of Hc components.

3. Uptake kinetics in aqueous – solid solution system

3.1. The unified uptake kinetics model (UUKM)

As we have shown previously (Thien et al., 2014), the common outcome from the surface entrapment model (SEMO, Watson, 2004) and the surface reaction kinetics model (SRKM, DePaolo, 2011) is that the fractionation coefficient $\Delta_{Tr,Hc}$ varies between two limits, $\Delta_{Tr,Hc,eq}$ and $\Delta_{Tr,Hc,ads} = F_{Tr} \cdot \Delta_{Tr,Hc,eq}$. The former limit is related to the (hypothetical) aqueous – solid solution equilibrium; the latter limit corresponds to the distribution of adsorbed Hc and Tr components in equilibrium with the same aqueous solution of constant composition. F_{Tr} is the so-called trace element enrichment/depletion factor.

These limits suggest that SRKM might be considered as an integrated and simplified form of SEMO, which assumes that the progressing precipitation tends to “entrap” the adsorbed layer composition, whereas the sub-surface layer dynamics (diffusivity) drives its composition to become closer to that in the assumed aqueous- solid solution equilibrium. Since the mineral continues to grow, the uptake of trace

elements in ‘older’ layers is, in principle, metastable. This irreversible process of enrichment or depletion of the solid with trace element relative to the expected aqueous– solid equilibrium concentration is called *surface entrapment*.

Fast precipitation augments the composition of the newly-grown layer (i.e. buried adsorbed layer) with the *Tr* content greater than expected from $\Delta_{Tr,Hc,eq}$ if *Tr* is hardly compatible with the host mineral structure ($F_{Tr} > 1$), and less than that if *Tr* is favoured by the bulk mineral lattice ($F_{Tr} < 1$). This enrichment or depletion can be counterbalanced by a concurrent partial release of the entrapped *Tr* back to aqueous solution.

Thus, one can assume that the apparent *Tr* sub-surface diffusivity D_s parameter in SEMO is related to the *Tr* backward rate parameter R_b in SRKM, defined through $v_b R_k = v_k R_b$. This assumption leads to the equality $v_k ml = D_s$ and further to the UUCM equation that predicts the effective fractionation coefficient $\Delta_{Tr,Hc}^*$:

$$\Delta_{Tr,Hc}^* = \Delta_{Tr,Hc,eq} \frac{D_s + R_{L,k} ml}{D_s + R_{L,k} ml / F_{Tr}} \quad (3.1)$$

where the mineral growth rate $R_{L,k}$ (eq 8) is taken in nm·s⁻¹. The enrichment parameter F_{Tr} can be, in principle, evaluated if both the *Hc-Tr* solid solution thermodynamic model and the surface complexation model for *Hc* and *Tr* components on the *Hc* surface is available. The D_s parameter is related to surface dynamics, roughness, and reactivity, and can only be assessed in the inverse modelling.

3.2. Uptake in seed-overgrowth solid solution phases

The setup of aqueous – solid solution uptake kinetics upon the host mineral growth, described in Section 2, has a shortcoming that the composition of the overgrowth is mixed or homogenized with that of the initial seed crystals phase (Fig. 3.1,A); it also cannot describe various cases of the (epitaxial) growth on surfaces of non-isostructural minerals. Therefore, it is desirable to have an option to link the specific surface and the kinetic rates for one “overgrowth” phase to the amount or surface of another “seed” or “substrate” phase; the latter may even be inert, or may have its own slow kinetics. This can be achieved with a *phase linkage*, in which the surface area of one “overgrowth” phase k is determined by the surface area of another (“substrate”) phase s (Fig. 3.1,B). If the linkage occurs via the surface area, the relationships between the surface area $A_{k,t}$ and the specific surface area $A_{S,k,t}$ become different from the usual ones as e.g. for the “substrate” phase where

$$A_{k,t} = A_{S,k,t} M_{M,k} n_{k,t} \quad (3.2)$$

However, in the case B (Fig. 3.1), this relationship holds constant for the “seed” phase:

$$A_s = A_{S,s} M_{M,s} n_s \quad (3.3)$$

For the “overgrowth” phase,

$$A_{k,t} = A_{S,k,t} (M_{M,k} n_{k,t} + M_{M,s} n_s). \quad (3.4)$$

In this case, in the specific surface correction (eq 2.7), the composite particle size, volume and mass are defined as

$$d_p = \frac{6(V_k + V_s)}{\psi_k A_k}; \quad V_p = \frac{1}{6}\pi d_p^3; \quad \text{and} \quad A_p = A_k \frac{V_p}{(V_k + V_s)}, \quad (3.5, 3.6)$$

respectively.

A similar concept of the *metastability chain* can be further used in thermodynamic modeling of adsorption and ion exchange. In this case, the adsorbed layer (solution) must be linked to the surface of the sorbent similar to the case (Fig. 3.1,B), but it has a limited thickness (total density). So, instead of growth or condensation, there will be a competition between surface species, described by the Langmuir or another adsorption isotherm.

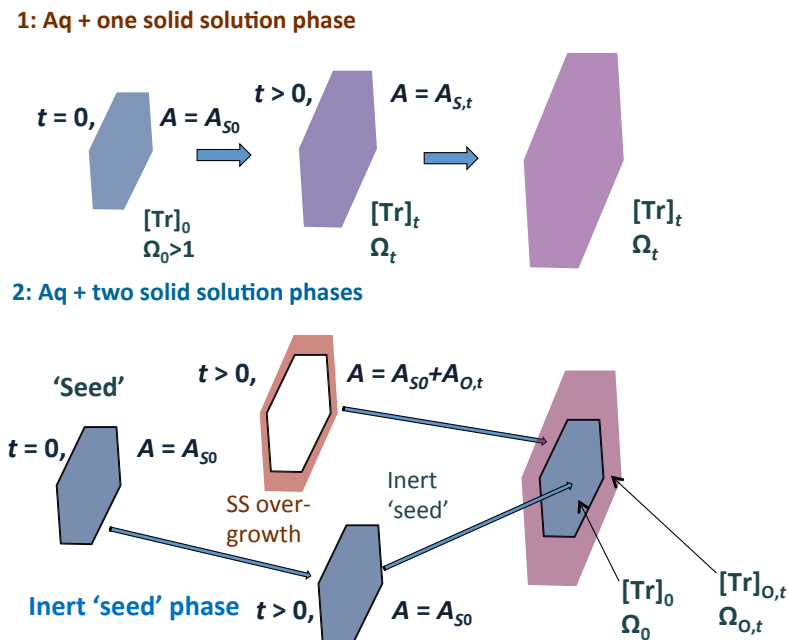


Figure 3.1. Schematic representation of two cases of aqueous-solid solution (Aq-SS) uptake: A – single solid solution phase; B – “overgrowth” phase on the surface of “seed” phase, to follow the overgrowth composition independently of the “seed” phase composition.

Example: For modelling trace element uptake in calcite, eq (3.1) can be combined with the empirical calcite precipitation rate law, for example from (Wolthers et al., 2012):

$$V_{Cal} = I^{-0.004} pH^{-10.71} \cdot \left(\frac{a_{Ca^{2+}}}{a_{CO_3^{2-}}} \right)^{-0.35} \cdot (\Omega^{0.5} - 1)^2 \quad (3.7)$$

where V_{Cal} is an average one-dimensional growth velocity (m/s). Assuming spherical particles of uniform size, it can be converted (Thien et al., 2013) into the net precipitation rate R_p (mol/m²/s):

$$R_p = \frac{V_{Cal}\rho_{Cal}}{3M_{Cal}} = \frac{10^6}{3} \frac{V_{Cal}}{V_{m,Cal}} = 9025.1 \cdot V_{Cal} \quad (3.8)$$

where M_{Cal} is the molar mass of the host mineral (g/mol), ρ_{Cal} is the host mineral density (g/m³), and $V_{m,Cal}$ is the molar volume in cm³/mol, $V_{m,cal} = 36.934$ cm³/mol). For seawater (diluted and undiluted), Wolthers et al. (2012) give a slightly different rate law to account for the inhibition effects of Mg²⁺ and other ions:

$$V_{Cal,SW} = I^{0.36} pH^{-10.99} \cdot \left(\frac{a_{Ca^{2+}}}{a_{CO_3^{2-}}} \right)^{-0.71} \cdot (\Omega^{0.5} - 2)^2 \quad (3.9)$$

The coefficient 9025.1 in eq (3.8) can be put on place of the «reaction» rate constant term $\left(\kappa_{k,r}^o \Lambda_{k,r} e^{\frac{-E_{k,r}}{RT}} \right)$ in eq (2.1). This makes the rate law (Wolthers et al. 2012) compatible with the “standard” TST kinetic rate law equation, presented in a general form in our implementation.

4. Modelling examples and verification

The idea of simulation tests was to show that the new functionality implemented in the TKinMet code library of GEMS3K code, as well as Phase and Process simulator modules of GEM-Selektor code, performs as desired. The simplest test example about portlandite shows how the seeded mineral growth is simulated, and why the proper shape factor function for the A_S correction is needed to fit the experimental data. The example for Caclite precipitation verifies the growth rate model (Wolthers et al., 2012) against the independent experiments. This rate model for calcite is used as a background in other test simulations aimed at showing how the UUKM equation (3.1) describes trace element uptake upon the host mineral growth, with important effects such as the impact of growth-rate variation and/or solution depletion.

4.1. Seeded growth of portlandite

This example shows a simulation of seeded precipitation of portlandite Ca(OH)₂ from aqueous solution at room temperature, with kinetic rate constant and shape factor parameterized against the experimental data (Tadros et al., 1976). These authors prepared supersaturated solutions by mixing equal volumes of 0.07 M CaCl₂ and 0.14 M NaOH stock solutions under CO₂-free conditions. In one series of experiments, the crystallization of portlandite was initiated by adding 10 mg of seed crystals with specific surface area $A_S = 2.1$ m²·g⁻¹ to 300 ml of the supersaturated solution. The time variation of the conductance was followed until constant conductance readings (achieved in 90 min or more). Plots of log(conductance at t – conductance at equilibrium) can be assumed proportional to log([Ca]_{aq,t} – [Ca]_{aq,eq}), provided that the Cl⁻ and Na⁺ concentrations remain constant during growth. Using this assumption, the initial [Ca]_{aq} = 0.0351 m, and the equilibrium [Ca]_{aq,eq} = 0.0231 m (Table 4.1), the conductance data from (Fig. 2 in Tadros et al., 1976) were converted into total dissolved [Ca]_{aq} values in a spreadsheet, with the estimated uncertainty < 0.3·10⁻³ m.

Table 4.1. Initial recipe of the chemical system “PortlKinExp” for the Process simulation

Property	Name	Quantity	Units	Comment
xa_	Aqua (H ₂ O)	299.26	g	Addition of 300 ml water H ₂ O at 1 bar, 25 C
xa_	CaCl ₂	0.0105	mol	Addition of 0.0105 moles of CaCl ₂ (in 150 ml of 0.07 M CaCl ₂ solution)
xa_	NaOH	0.021	mol	Addition of 0.021 moles of NaOH (in 150 ml of 0.14 M NaOH solution)
xd_	Portlandite	0.01	g	Addition of 10 mg Ca(OH) ₂ “seed” crystals
bi_	Nit	0.0016	mol	Addition of atmospheric nitrogen
bi_	O	0.0004	mol	Addition of oxygen (to form a CO ₂ -free atmosphere)
dul_	Portlandite	0.000135	mol	Upper AMR for 10 mg of “seed” portlandite

“Property” identifies an entry in the GEM-Selektor Recipe dialog.

Model calculations were performed using the GEM-Selektor v.3.3 code prototype, in the “Kinetics” test modeling project, at $P=1$ bar, $T=25$ C. The initial system recipe was set as given in Table 4.1; The Davies equation was used for computing aqueous activity coefficients. The input thermodynamic data were taken from the GEMS version of the PSI-Nagra database 01/07 (Thoenen, 2012; <http://gems.web.psi.ch/TDB>). The GEM-calculated initial saturation index of portlandite was 2.836, the total dissolved $[Ca]_{aq} = 0.0351$ m. In a separate GEM calculation of equilibrium in the same system without the upper AMR for portlandite, $[Ca]_{aq,eq}$ was found to be equal to 0.0231 m.

Kinetic parameters of Portlandite phase were set according to a simple zero-order rate equation

$R_{Port} = \kappa_{Port}^{-} (1 - \Omega_{Port})$. The rate constant value κ_{Port}^{-} together with the dependence of the sphericity factor ψ_{Port} on saturation index given as $\psi_{Port}(t) = \psi_0 + \psi_1 u$ where $u = \log_{10} \Omega_{Port,t}$, was adjusted in trial-and-error process simulations using CEM-Selektor Process module and Graphics dialog.

The time interval was [0; 6000] s with time step Δt of 15 or 30 s; no visible differences on the model curves were found with these time stepping. Excellent fit to experimental conductivity data (Fig. 4.1) was obtained with parameters given in Table 4.2.

Table 4.2. Parameters of the kinetic model for portlandite seeded growth.

Parameter	Value	Comment
Net rate constant at 25 C κ_{Port}^{-} (mol·m ⁻² ·s ⁻¹)	-3.23·10 ⁻⁵	Fit to data
Arrhenius factor Λ_{Port}	1.0	Default
Activation energy E_{Port}	0	Default
Reactive surface area fraction θ_{Port}	1.0	Default
Sphericity factor dependence $\psi_0 + \psi_1 u$: ψ_0	0.83	Geometry;
	ψ_1	fit to data
Initial specific surface area $A_{S,Port,0}$ (m ² ·g ⁻¹)	2.1	experiment
Initial portlandite “seed” mass m_{Port} (g)	0.01	experiment

For comparison, Fig. 4.1 shows a simulation run with the same parameters, but without the correction of shape factor (sphericity), kept constant at its “equilibrium” value of 0.83. This shows that a significant change in morphology of portlandite particles must take place during early stages of growth. This is indirectly corroborated by (Tomazic et al. 1986) who provide the evidence of morphology changes upon portlandite precipitation.

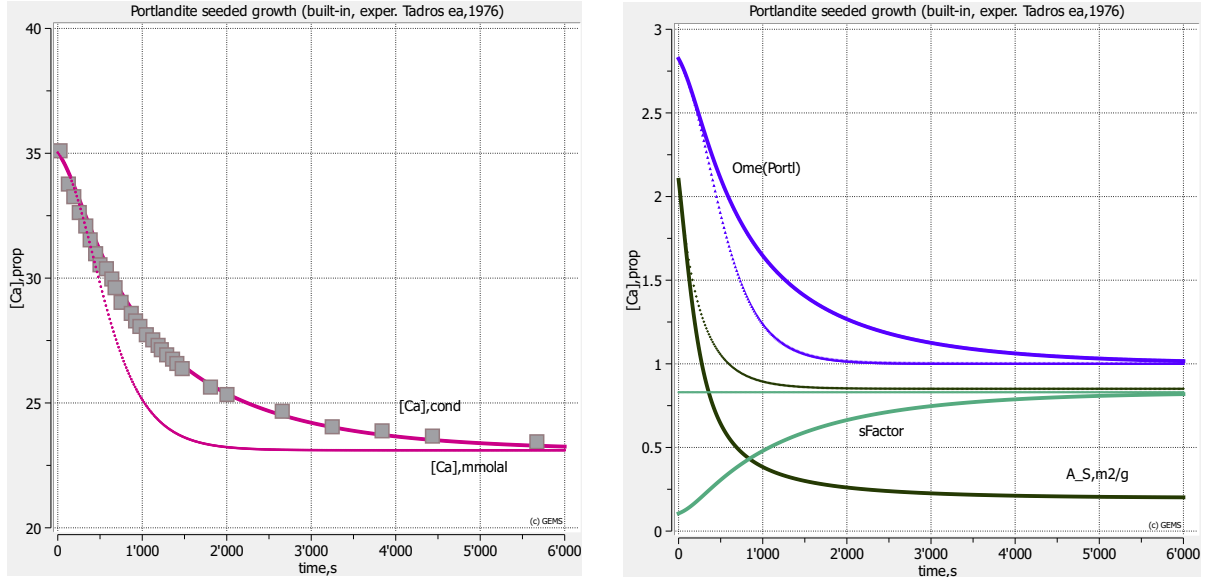


Figure 4.1. Simulation of seeded growth of portlandite (dense curves) in comparison with experimental data from (Tadros et al., 1976) (squares) and another simulation with constant $sFactor$ (sphericity factor) $\psi_{Port} = 0.83$ (thin dotted curves). $Ome(Port)$ denotes $\Omega_{Port,t}$.

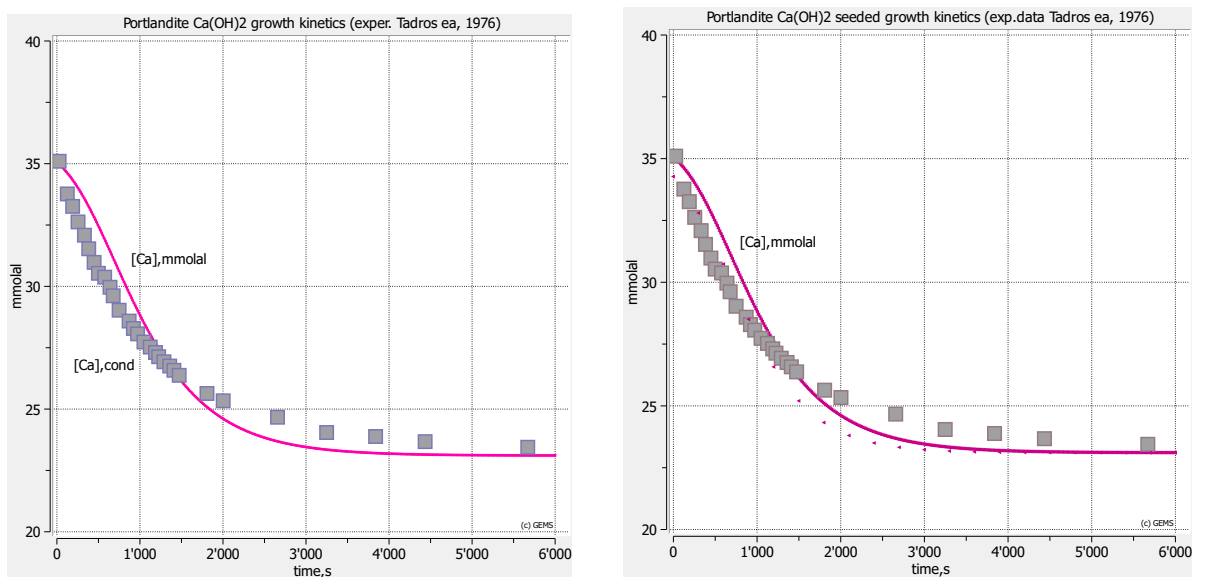


Figure 4.2. Sensitivity of kinetic simulations of seeded growth of portlandite. Left-hand side: “best fit” with $\psi_{Port} = 1.0$, $\kappa_{Port}^- = -2.1 \text{ mol} \cdot \text{m}^{-2} \cdot \text{s}^{-1}$, and $\Delta t = 15$ or 30 s. Right-hand side: the same model run compared with the one at time stepping of $\Delta t = 300$ s (dots).

Some other model sensitivity cases are given in Fig. 4.2, on the left side of which the “best” fit at constant $\psi_{Port} = 1.0$ and $\kappa_{Port}^- = -2.1 \text{ mol}\cdot\text{m}^{-2}\text{s}^{-1}$ shows that the absence of shape factor correction results in a wrong shape of the model curve that cannot be fixed by adjusting the rate constant alone. The right side shows the impact of too large time step duration. Finding the optimal time stepping is not a trivial issue that requires more investigation. Presently, the practical rule would be to demonstrate that the same model curve is produced with two different (small enough) time step length values.

5.2. Calcite precipitation

For modelling kinetics of trace element uptake in calcite, eq (3.1) must be combined with the calcite precipitation rate law. We used the rate law ($T=20 \text{ C}$) from (Wolthers et al., 2012):

$$R_{L,Cal} = I^{-0.004} pH^{-10.71} \cdot \left(\frac{a_{Ca^{2+}}}{a_{CO_3^{2-}}} \right)^{-0.35} \cdot (\Omega^{0.5} - 1)^2 \quad (4.1)$$

where $R_{L,Cal}$ is the average orthogonal surface propagation velocity (in $\text{m}\cdot\text{s}^{-1}$). It can be converted into the net precipitation rate R_{Cal} (in $\text{mol}\cdot\text{m}^{-2}\cdot\text{s}^{-1}$):

$$R_{Cal} = 10^6 \frac{R_{L,Cal}}{V_{M,Cal}} = 27075.3 \cdot R_{L,Cal} \quad (4.2)$$

where $V_{M,Cal} = 36.934 \text{ cm}^3\cdot\text{mol}^{-1}$ is the calcite molar volume. For seawater (diluted and undiluted), Wolthers et al. (2012) proposed a slightly different rate law to account for the inhibition effects of Mg^{2+} and other ions:

$$R_{L,Cal,SW} = I^{0.36} pH^{-10.99} \cdot \left(\frac{a_{Ca^{2+}}}{a_{CO_3^{2-}}} \right)^{-0.71} \cdot (\Omega^{0.5} - 2)^2 \quad (4.3)$$

The activation energy of calcite growth is $48.1 \text{ kJ}\cdot\text{mol}^{-1}$ at $T=25 \text{ C}$ (Inkseep and Bloom, 1985). This yields the Arrhenius constant $\Lambda_{k,r} = 1 \cdot e^{\frac{-E_{k,r}^*}{R \cdot 298.15}} = 2.6706 \cdot 10^8$ leading to a temperature correction factor from 298 to 293 K equal to 0.7163. Coefficient $-27075.3/0.7163 = -37800$ can now be put in place of the rate constant κ_{Cal}^- used in our “standard” eq (1.2).

Let us check this rate equation on an example for seeded precipitation of calcite CaCO_3 from aqueous solution at $T = 10 \text{ C}$, compared with the experimental data (Dreybrodt et al. 1997). These authors prepared supersaturated solutions by dissolving CaCO_3 powders and CO_2 in deionized water. Immediately after filling the vessel with the supersaturated solution ($4 \cdot 10^{-3} \text{ M} [\text{Ca}^{2+}]$), 3.16 mmol of calcite seed (with $A_{S,0} = 0.184 \text{ m}^2\cdot\text{g}^{-1}$) was introduced. Because of calcite precipitation, $[\text{Ca}^{2+}]$ (monitored by conductance measurements) decreased with time tending toward the equilibrium $[\text{Ca}^{2+}]$ value of $2.8 \cdot 10^{-3} \text{ M}$.

Model calculations at 1 bar, 10°C were performed in the “Kinetics” test modeling project using the GEM-Selektor v.3.3 prototype. The Davies equation was used for computing aqueous activity coefficients. Thermodynamic data were taken from the GEMS version of the PSI-Nagra database 01/07 (Thoenen, 2012; <http://gems.web.psi.ch/TDB>). The initial system recipe is given in Table 4.3. GEM calculation for this system yields the initial saturation index of calcite ($\log_{10}\Omega_{Cal} = 2.53$). Note that this system is extremely sensitive to the initial addition of CO_2 to bulk composition. The value in Table 4.3 was found by trial-and-error to set calculated $\text{pCO}_2 = 0.001 \text{ bar}$ as mentioned by Dreybrodt et al. (1997).

Table 4.3. Initial recipe of the chemical system “Calcite” for the GEM process simulation

Property	Name	Quantity	Units	Comment
xa_	Aqua	262	g	Addition of 262 ml water H ₂ O at 1 bar, 10°C
xa_	CaCO ₃	0.00435	mol	Addition of 0.00435 moles of CaCO ₃ for both the solution and the seed calcite.
xa_	CO ₂	0.0011	mol	Addition of 0.011 moles of CO ₂ to obtain pCO ₂ = 1·10 ⁻³ bar (adjusted by trial-end-error)
xa_	O ₂	1·10 ⁻⁶	mol	Addition of O ₂ to stabilize redox state
dll_	Calcite	0.00316	mol	Lower AMR for 0.00316 mol of “seed” calcite
dul_	Calcite	0.00316	mol	Upper AMR for 0.00316 mol of “seed” calcite

Kinetic parameters in the Calcite phase record were set according to Table 4.4. The sphericity factor of calcite was set constant at $\psi_{Cal} = 0.8$. Process simulations were performed within the time interval [0; 44000] s with time step $\Delta t = 10$ s (Fig. 4.3).

The model reproduces well the measured [Ca²⁺] at times longer than 8000 s. Some deviation at shorter times curve shape may be due the “seed” sample heterogeneity or variation in particle morphology upon growth, which are not accounted for in the kinetic model. In general, a good fit to experimental data without any adjustment of kinetic parameters confirms the validity of calcite growth kinetic rate equation (Wolthers et al., 2012), especially at close-to-equilibrium conditions and slow rates.

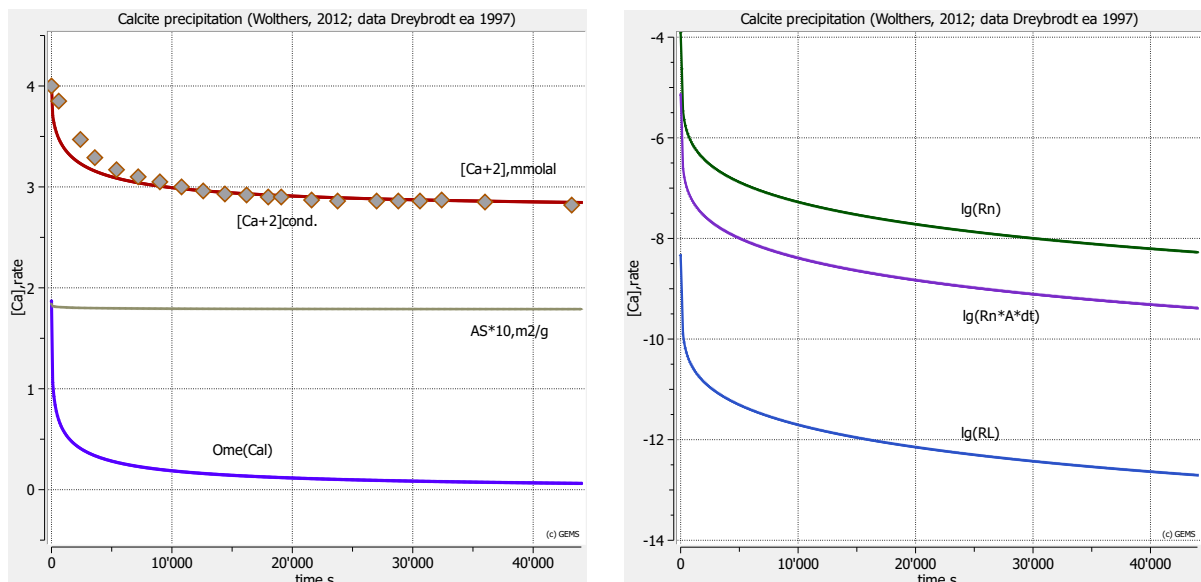


Figure 4.3. Simulations of calcite precipitation with kinetic parameters from Table 4.4. Calcite specific surface area AS*10 is 10·A_{S,cal} in m²·g⁻¹. Ome(Cal) is the current stability index Ω_{Cal} of calcite. Decimal logarithmic rates (right-hand side) are shown in mol·m⁻²·s⁻¹ (Rn); in moles per time step (Rn*A*dt); and in m·s⁻¹ (RL).

Table 4.4. Parameters of the kinetic rate model for calcite precipitation

Comment	Value	Reference
Net rate constant at 25°C κ_{Cal}^- (mol·m ⁻² ·s ⁻¹)	-37800	See text
Arrhenius factor Λ_{Cal}	$2.671 \cdot 10^8$	See text
Activation energy E_{Cal} (kJ·mol ⁻¹)	48.1	(Inkseep and Bloom 1985)
Reactive surface fraction θ_{Cal}	1.0	Default
Sphericity factor ψ_{Cal}	0.8	Geometry (as for cube)
Initial specific surface area $A_{S,Cal,0}$ (m ² ·g ⁻¹)	0.184	Experiment
Initial calcite “seed” mass (g)	0.316	Experiment

4.3. Simulations of Sr and Cd uptake kinetics in calcite

In this example for seeded co-precipitation of “incompatible cation” Sr²⁺ in calcite CaCO₃ from aqueous solution, the uptake kinetics model has been parameterized against the experimental data by (Lorens 1981). In this experiment, the precipitation of calcite was triggered by a constant addition of Na₂CO₃ stock solution with a rate $2.16 \cdot 10^{-8}$ mol·s⁻¹ to the initial solution, which induced an average calcite growth rate of $2.94 \cdot 10^{-6}$ mol·m⁻²·s⁻¹.

Simulations have been performed using the GEM-Selektor v.3.3 code prototype, in the “LorensSrCa” test-modeling project, at 1 bar, 25°C. The initial system recipe is given in Table 4.5; the extended Debye-Hückel equation was used for aqueous activity coefficients. The input thermodynamic data were taken from the GEMS version of PSI-Nagra database 01/07.

A solid-solution phase Calcite-Sr_ovg consisted of two end-members, Cal (calcite) and SrCO₃-cal (SrCO₃ with calcite structure), and a regular parameter $W_G = 4.4$ kJ·mol⁻¹ (Kulik et al. 2010). This solid solution phase was initially used without AMRs to calculate the equilibrium fractionation coefficient $\Delta_{Sr,Ca,eq}=0.021$; the recipe of the initial system is provided in Table 4.5. Kinetic rate parameters for the Calcite-Sr_ovg phase were taken the same as in Table 4.4; the UUKM parameters were set according to Table 4.6. The Calcite-Sr_ovg phase was linked to the surface area of the Calcite_seed pure phase, with initial $A_{S,Cal}=0.8$ m²·g⁻¹.

A first Process simulation has been run within the time interval [0; 540] s (actual duration of the experiment) with time step of 1 s. To explore potential depletion effects, the second simulation has been performed within a hypothetical longer time interval [0; 10000] s. The results are shown in Fig. 4.4. They indicate a similar enrichment of Sr in over-grown calcite as in the experiments (Lorens, 1981), whereas at long reaction time, the aqueous solution depletion effect drives the effective Sr fractionation coefficient back to its aqueous-solid solution equilibrium value (0.021) and then to much lower values.

Table 4.5. Recipe of initial chemical system “SrCaLorens7” for the Process simulation

Property	Name	Quantity	Units	Comment
xa_	Aqua	150	g	Addition of 150 ml water H ₂ O at 1 bar, 25°C
xa_	NaCl	0.1035	mol	Addition of 0.1035 moles of NaCl
xd_	NaHCO ₃	0.0145	mol	Addition of 0.0145 moles of NaHCO ₃
xa_	CaCl ₂	0.0015	mol	Addition of 0.0015 moles of CaCl ₂
xa_	Na ₂ CO ₃	1·10 ⁻⁷	mol	Addition of 1·10 ⁻⁷ moles of Na ₂ CO ₃
xa_	CaCO ₃	9.2·10 ⁻⁵	mol	Addition of 9.2·10 ⁻⁵ moles of CaCO ₃ for seed
xd_	Sr+2	4.59·10 ⁻⁸	mol	Addition of 4.59·10 ⁻⁸ moles of SrCl ₂
xd_	Cl-	9.18·10 ⁻⁸	mol	Addition of 4.59·10 ⁻⁸ moles of SrCl ₂
xa_	CO ₂	0.055	mol	Addition of CO ₂ to equilibrate the solution
xa_	O ₂	0.1	g	Addition of O ₂ to set redox state
xa_	N ₂	3	g	Addition of N ₂ to equilibrate the solution
dll_	Cal_seed	9.2·10 ⁻⁵	mol	Lower AMR set for “seed” calcite
dul_	Cal_seed	9.2·10 ⁻⁵	mol	Upper AMR set for “seed” calcite

Process simulation: titration by adding Na₂CO₃ with a rate 2.16·10⁻⁸ mol·s⁻¹.

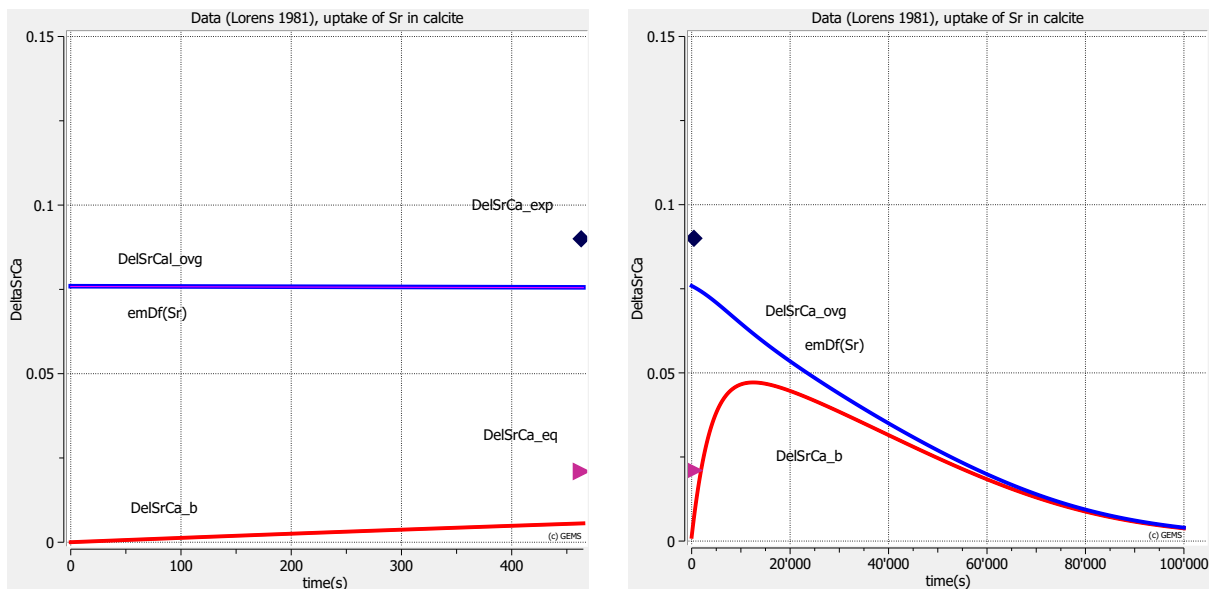


Figure 4.4. Simulations of time-dependent uptake of Sr in calcite (different time scales on left- and right-hand sides). DelSrCa_exp: experimental $\Delta_{Sr,Ca}$; DelSrCa_eq: aqueous – solid solution equilibrium $\Delta_{Sr,Ca,eq}$; emDf(Sr): effective $\Delta_{Sr,Ca}$; DelSrCa_ovg: average $\Delta_{Sr,Ca}$ in the overgrowth phase; DelSrCa_b: bulk $\Delta_{Sr,Ca,eq}$ in the seed + overgrowth phase.

Table 4.6. Parameters of the uptake kinetic model for Sr in calcite

Comment	Value	Reference
Initial specific surface area $A_{S,0}$ ($\text{m}^2 \cdot \text{g}^{-1}$)	0.8	experiment
Initial calcite “seed” mass (g)	$9.2 \cdot 10^{-3}$	experiment
Surface enrichment factor F_{Sr}	6.2	(Thien et al., 2014)
Equilibrium fractionation coefficient $\Delta_{\text{Sr,Ca},eq}$	0.021	(Kulik et al., 2010)
Sr sub-surface diffusivity $D_{s,\text{Sr}}$ ($\text{nm}^2 \cdot \text{s}^{-1}$)	0.02	(Thien et al., 2014)
Sr lattice diffusivity in calcite $D_{l,\text{Sr}}$ ($\text{nm}^2 \cdot \text{s}^{-1}$)	$1 \cdot 10^{-16}$	the same
Length l at which DS applies in the subsurface layer (nm)	0.5	the same
Length multiplicator m	6	the same

In another example, the seeded precipitation of “compatible element” cadmium with calcite at 1 bar, 25 C has been simulated and compared with the experimental data (Lorens, 1981). As in the previous example, the process is driven by constant addition of Na_2CO_3 at the rate $8.37 \cdot 10^{-9} \text{ mol} \cdot \text{s}^{-1}$ that induces the average growth rate $2.975 \cdot 10^{-6} \text{ mol} \cdot \text{m}^{-2} \cdot \text{s}^{-1}$ of calcite.

Simulations have been performed in the “CdCalcite” test modeling project. The initial system recipe was set as given in Table 4.7; the Debye-Hückel equation was used for computing aqueous activity coefficients. The input thermodynamic data were used from the GEMS version of the PSI-Nagra database 01/07; those for otavite CdCO_3 - from (Gamsjäger et al., 1999); and for Cd aqueous species – from the SUPCRT database (built-in in GEM-Selektor).

A solid-solution phase Calcite-Ota_ovg consists of two end-members, Cal (calcite) and Otavite (CdCO_3), with the regular interaction parameter $W_G = 2.975 \text{ kJ mol}^{-1}$ (Tesoriero and Pankow, 1996). This solid solution phase was initially used without AMRs to calculate the equilibrium fractionation coefficient $\Delta_{\text{Cd,Ca},eq}=33.0$; the recipe of the initial system is provided in Table 4.7. Kinetic rate parameters for the Calcite-Ota_ovg phase were taken the same as in Table 4.4; the UUKM parameters were set according to Table 4.8. The Calcite-Ota_ovg phase was linked to the surface area of the Calcite_seed pure phase, with initial $A_{S,Cal}=0.8 \text{ m}^2 \cdot \text{g}^{-1}$.

Table 4.7. Recipe of initial chemical system “CdCaLorens2” for the Process simulation

Property	Name	Quantity	Units	Comment
xa_	Aqua	150	g	Addition of 150 ml water H_2O at 1 bar, 25°C
xa_	NaCl	0.1035	mol	Addition of 0.1035 moles of NaCl
xd_	NaHCO_3	0.0017	mol	Addition of 0.0017 moles of NaHCO_3
xa_	CaCl_2	0.0015	mol	Addition of 0.0015 moles of CaCl_2
xa_	CaCO_3	$3.1 \cdot 10^{-5}$	mol	Addition of $3.1 \cdot 10^{-5}$ moles of CaCO_3 for seed
xd_	Cd+2	$1 \cdot 10^{-6}$	mol	Addition of $1 \cdot 10^{-6}$ moles of CdCl_2
xd_	Cl^-	$2 \cdot 10^{-6}$	mol	Addition of $2 \cdot 10^{-6}$ moles of CdCl_2
xa_	CO_2	0.043	mol	Addition of CO_2 to equilibrate the solution
xa_	O_2	0.1	g	Addition of O_2 to equilibrate the solution
xa_	N_2	2	g	Addition of N_2 to equilibrate the solution
dll_	Cal_Seed	$3.1 \cdot 10^{-5}$	mol	Lower AMR for $3.1 \cdot 10^{-3}$ g of “seed” calcite
dul_	Cal_Seed	$3.1 \cdot 10^{-5}$	mol	Upper AMR for $3.1 \cdot 10^{-3}$ g of “seed” calcite
dul_	Cal	$1 \cdot 10^{-10}$	mol	Upper AMR for $1 \cdot 10^{-10}$ mol of calcite end member
dul_	Otavite	$1 \cdot 10^{-12}$	mol	Upper AMR for $1 \cdot 10^{-12}$ mol of otavite end member

Table 4.8. Parameters of the uptake kinetic model for Cd in calcite

Comment	Value	Reference
Initial specific surface area $A_{S,0}$ ($\text{m}^2 \cdot \text{g}^{-1}$)	0.8	experiment
Initial calcite “seed” mass (g)	$3.1 \cdot 10^{-3}$	experiment
Surface enrichment factor F_{Cd}	0.3	(Thien et al., 2014)
Equilibrium fractionation coefficient $\Delta_{Cd,Ca,eq}$	33.0	(Tesoriero and Pankow, 1996)
Cd sub-surface diffusivity $D_{s,Cd}$ ($\text{nm}^2 \cdot \text{s}^{-1}$)	0.02	(Thien et al., 2014)
Cd lattice diffusivity in calcite $D_{l,Cd}$ ($\text{nm}^2 \cdot \text{s}^{-1}$)	$1 \cdot 10^{-16}$	the same
Length l at which D_S applies in the subsurface layer (nm)	0.5	the same
Length multiplicator m	6	the same

A first Process simulation has been run within the time interval [0; 1200] s (actual duration of the experiment) with time step of 10 s. To explore the potential aqueous solution depletion effects, the second simulation has been run within a longer time interval [0; 100000] s with time step of 100 s. The results are shown in Fig. 5.5. They indicate the same depletion of Cd in over-grown calcite as observed in the experiments (Lorens, 1981), whereas at long reaction times, the aqueous solution depletion effect would drive the effective Cd fractionation coefficient up to its aqueous-solid solution equilibrium value and then to much higher values.

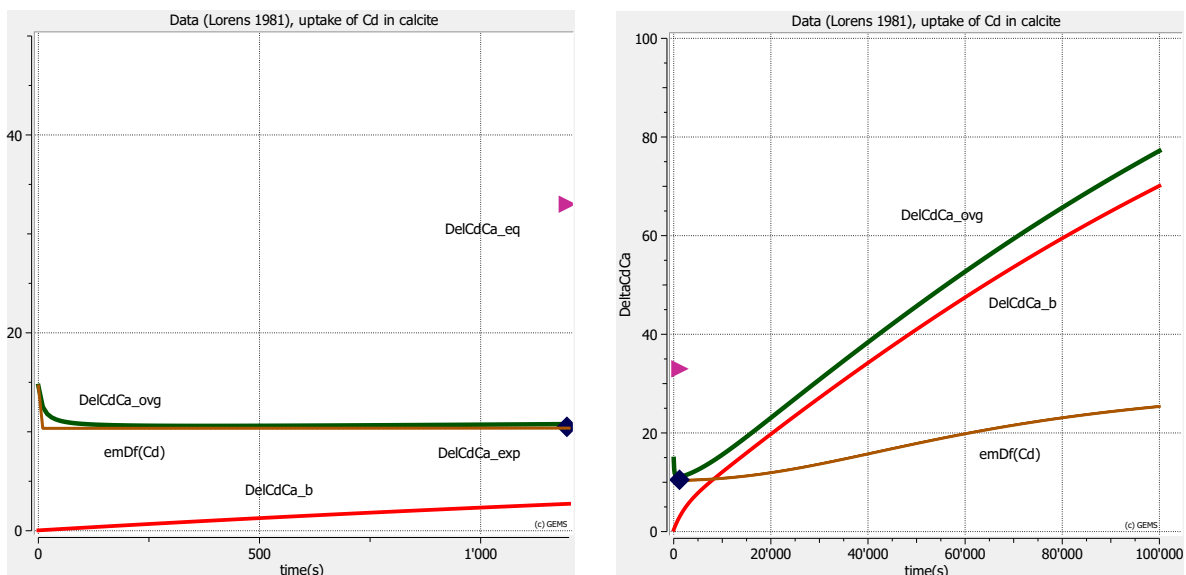


Figure 4.5. Simulations of time-dependent uptake of Cd in calcite (different time scales on left- and right-hand sides). $\text{DelCdCa}_{\text{exp}}$: experimental $\Delta_{\text{Cd,Ca}}$; $\text{DelCdCa}_{\text{eq}}$: aqueous – solid solution equilibrium $\Delta_{\text{Cd,Ca},\text{eq}}$; $\text{emDf}(\text{Cd})$: effective $\Delta_{\text{Cd,Ca}}$ (eq 18); $\text{DelCdCa}_{\text{ovg}}$: average $\Delta_{\text{Cd,Ca}}$ in the overgrowth phase; $\text{DelCdCa}_{\text{b}}$: bulk $\Delta_{\text{Sr,Ca},\text{eq}}$ in the seed + overgrowth phase.

4.4. Simulation of Sr uptake in calcite from seawater –air system

The idea of this example was to demonstrate potentially complex uptake processes on the background of temperature, composition change, and depletion effects in aqueous- solid solution systems that can be modeled with the new TKinMet code functionality. The obtained predictions may comprise a challenge for future experimental verifications. We also compare both one- and two- solid solution cases as outlined in Fig. 3.1.

One solid solution case. The initial chemical system “Sr-calcite” was set in the “CarbSea” test modeling project, using the recipe in Table 4.5 and the extended Debye-Hückel equation with common size parameter for aqueous activity coefficients. The input thermodynamic data was taken from the GEMS version of the PSI-Nagra database 01/07, as in other examples.

The solid-solution phase Calcite-Sr_ovg with two end-members, Cal (calcite) and SrCO₃-cal (SrCO₃ with calcite structure), and a regular parameter $W_G = 4.4 \text{ kJ}\cdot\text{mol}^{-1}$ was included into the system definition. This phase model is the same as that considered in Section 5.3 above. Kinetic rate parameters for the Calcite-Sr_ovg phase were taken the same as in Table 4.4; the UUKM parameters were set as in Table 4.9, except that initial $A_{S,0}$ set equal to 0.09 m²·g⁻¹. In Fig. 4.6, the results of simulations at $P=1$ bar, $T=25$ C and 15 C are presented.

Table 5.9. Recipe of initial chemical system “SrCalcite” for the Process simulation

Property	Name	Quantity	Units	Comment
xa_	Aqua	965	g	Addition of H ₂ O to produce 1 kg of seawater
xa_	AtmAirNit	10	kg	Atmosphere (pCO ₂ = 36 Pa)
xa_	CaCO ₃	1.0·10 ⁻⁴	mol	Addition of 0.1 mmoles of CaCO ₃ for seed
xd_	SeaSalt	35	g	Addition of 35 g normative sea salt
dul_	Cal	1.001·10 ⁻⁴	mol	Upper AMR set for 10 mg·kgw ⁻¹ “seed” calcite
dul_	SrCO ₃ -cal	1.8·10 ⁻¹⁰	mol	Upper AMR set for trace Sr content in “seed” calcite

Process simulation: titration by adding Na₂CO₃ with a rate of 0.05 mmol per hour; time interval: [0; 200] h; time step $\Delta t = 1$ h. Normative sea salt composition (in mmol·kgw⁻¹, without H₂O):

C	1.93895	Mg	54.9493
Ca	10.6366	Na	484.336
Cl	565.497	O	123.597
H	2.339	S	29.1959
K	10.5568	Sr	0.09308

The linked two-solid-solutions case. The initial chemical system “Sr-calc-ovg” was set in the “CarbSea” test modeling project, using the recipe in Table 4.5 and other features similar to the previous case. Two solid solution phases were included. The “seed” ArgStr phase with end members Arg (aragonite) and Str (strontianite) and properties from (Kulik et al., 2010); the amount of Arg was fixed by lower and upper AMRs at 0.0001 mol, and the amount of Str end member fixed by AMRs at 10⁻⁹ mol; initial specific surface area was $A_{S,0} = 0.09 \text{ m}^2\cdot\text{g}^{-1}$. The “overgrowth” solid-solution phase Calcite-Sr_ovg with end-members, Cal (calcite) and SrCO₃-cal (SrCO₃ with calcite structure) was the same as in the previous case, except that it was linked to the surface of the “seed” phase. The time step and interval were the same as before.

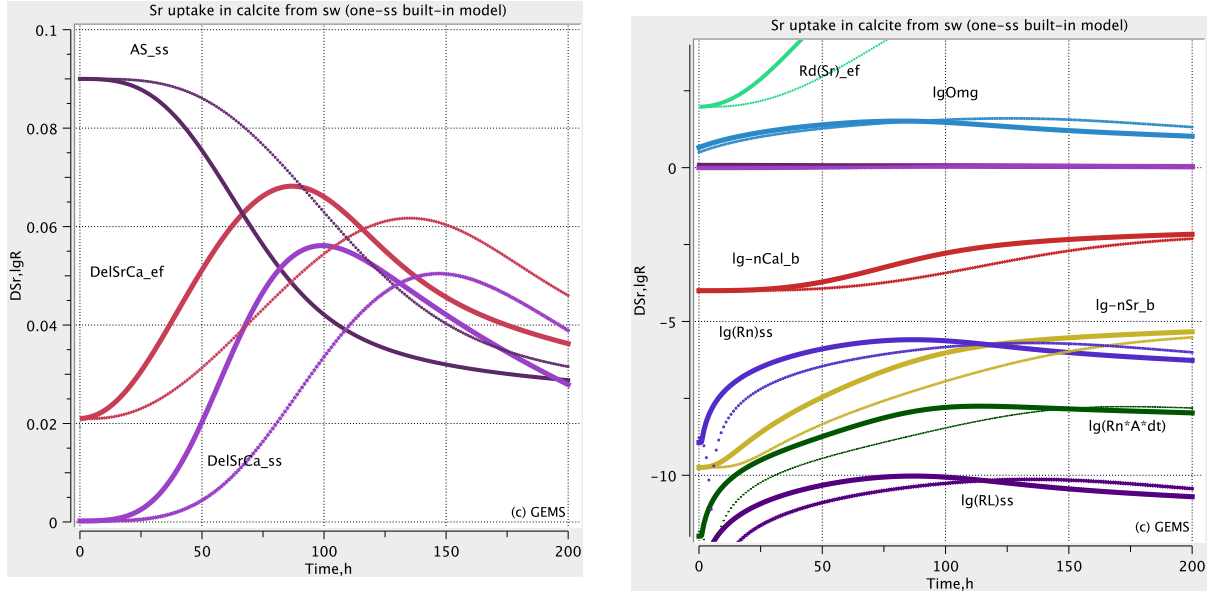


Figure 4.6. Simulation runs for one-phase case of Sr uptake in calcite from seawater, showing the effects of temperature (thick curves: $T=25\text{ C}$, thin dotted curves: $T=15\text{ C}$), varying precipitation rate, and seawater depletion. $\Delta_{\text{Sr},\text{Ca}}\text{ef}$: effective $\Delta_{\text{Sr},\text{Ca}}$; $\Delta_{\text{Sr},\text{Ca}}\text{ss}$: bulk $\Delta_{\text{Sr},\text{Ca}}$ in solid solution phase; $AS\text{ss}$: specific surface area; $lgOmg$: saturation index; $nCal_b$ and nSr_b : amounts of end members; Rn , RL and Rn^*A^*dt : precipitation rates in $\text{mol}\cdot\text{m}^{-2}\cdot\text{s}^{-1}$, $\text{m}\cdot\text{s}^{-1}$, and mol per time step, respectively.

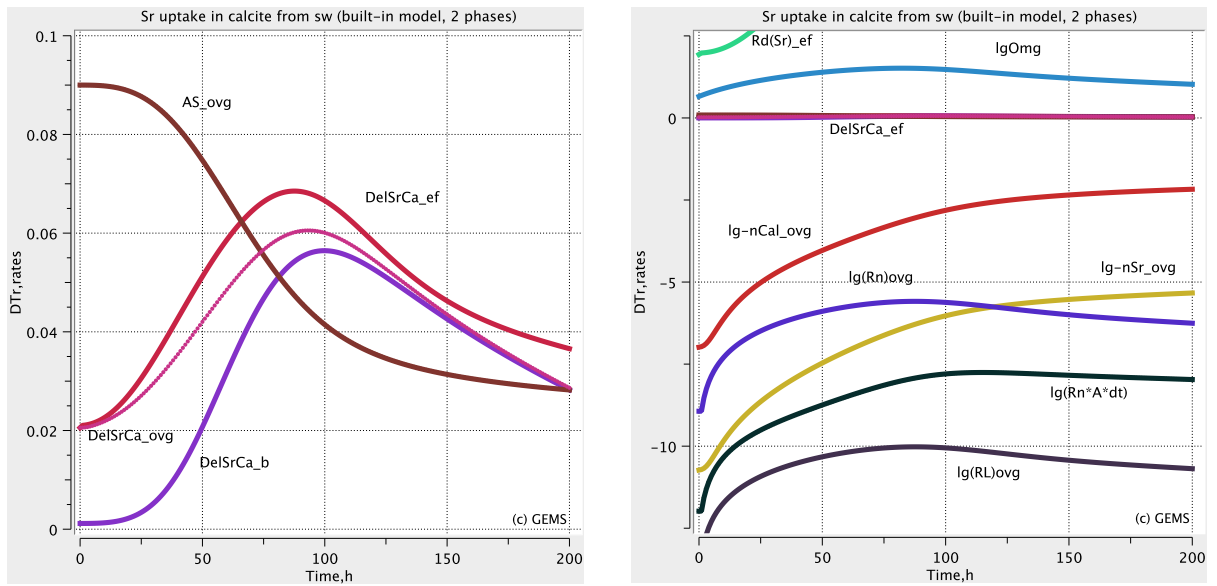


Figure 4.7. Simulation runs for linked two-phase case of Sr uptake in calcite from seawater at $P=1\text{ bar}$, $T=25\text{ C}$, showing the effects of varying precipitation rate, and seawater depletion. $\Delta_{\text{Sr},\text{Ca}}\text{ef}$: effective $\Delta_{\text{Sr},\text{Ca}}$; $\Delta_{\text{Sr},\text{Ca}}\text{ovg}$: $\Delta_{\text{Sr},\text{Ca}}$ in "overgrowth" solid solution phase; $\Delta_{\text{Sr},\text{Ca}}\text{b}$: bulk $\Delta_{\text{Sr},\text{Ca}}$ in the solid; $AS\text{ovg}$: specific surface area of the "overgrowth"; $lgOmg$: saturation index; $nCal\text{ovg}$ and $nSr\text{ovg}$: amounts of end members of the "overgrowth" phase; Rn , RL and Rn^*A^*dt : precipitation rates.

The simulation results for this case are shown in Fig. 4.7, where the variation of amount and composition of the “overgrowth” phase can now be followed separately from the “seed” phase. The variation of “bulk solid” Sr fractionation coefficient is clearly the same as in the single phase case at the same temperature: it increases by factor 3 or more at maximum calcite growth rate, then decreases due to depletion of the aqueous solution.

References

- DePaolo D. J. (2011). Surface kinetic model for isotopic and trace element fractionation during precipitation of calcite from aqueous solutions. *Geochimica et Cosmochimica Acta* **75**, 1039-1056.
- Dreybrodt W., Eisenlohr L., Madry B., and Ringer S. (1997). Precipitation kinetics of calcite in the system CaCO₃-H₂O-CO₂: The conversion to CO₂ by the slow process H⁺+HCO₃⁻ → CO₂+H₂O as a rate limiting step. *Geochimica et Cosmochimica Acta* **49**, 2165-2180.
- Fritz B., Clement A., Amal Y., and Noguera C. (2009). Simulation of the nucleation and growth of simple clay minerals in weathering processes: The NANOKIN code. *Geochimica et Cosmochimica Acta* **73**, 1340-1358.
- Gamsjäger H., Preis W., Königsberger E., Magalhaes M. C. and Brandao P. (1999). Solid-solute phase equilibria in aqueous solution. XI. Aqueous solubility and standard Gibbs energy of cadmium carbonate. *Journal of Solution Chemistry* **28**, 711-720.
- Glynn P. and Reardon E.J. (1990). Solid-solution aqueous-solution equilibria: Thermodynamic theory and representation. *American Journal of Science* **290**, 164-201.
- Hellmann R. and Tisserand D. (2006). Dissolution kinetics as a function of the Gibbs free energy of reaction: An experimental study based on albite feldspar. *Geochimica et Cosmochimica Acta* **70**, 364-383.
- Inskeep W.P. and Bloom P.R. (1985). An evaluation of rate equations for calcite precipitation kinetics at PCO₂ less than 0.01 atm and pH greater than 8. *Geochimica et Cosmochimica Acta* **49**, 2165-2180.
- Karpov I.K., Chudnenko K.V., Kulik D.A., Avchenko O.V., and Bychinskii, V.A. (2001). Minimization of Gibbs free energy in geochemical systems by convex programming. *Geochemistry International* **39**, 1108-1119.
- Kulik D.A., Wagner T., Dmytrieva S.V., Kosakowski G., Hingerl F.F., Chudnenko K.V., and Berner U. (2013). GEM-Selektor geochemical modeling package: revised algorithm and GEMS3K numerical kernel for coupled simulation codes. *Computational Geosciences* **17**, 1-24.
- Kulik D. A., Vinograd V. L., Paulsen N., and Winkler, B. (2010). (Ca,Sr)CO₃ aqueous-solid solution systems: From atomistic simulations to thermodynamic modelling. *Physics and Chemistry of the Earth* **35**, 217-232.
- Lasaga A.C. (1998). Kinetic theory in the Earth sciences. Princeton University Press, Princeton NJ.
- Lorens R. B. (1981). Sr, Cd, Mn and Co distribution coefficients in calcite as a function of calcite precipitation rate. *Geochimica et Cosmochimica Acta* **45**, 553-561.
- Madé B., Clement A., and Fritz B. (1994). Computers and Geosciences **20**, 1347-1363.
- Marini L., Ottonello G., Canepa M., and Cipolli F. (2000). Water-rock interaction in the Bisagno valley (Genoa, Italy): Application of an inverse approach to model spring water chemistry. *Geochimica et Cosmochimica Acta* **64**, 2617-2635.
- Mironenko M.V. and Zolotov M.Yu. (2012). Equilibrium–kinetic model of water–rock interaction. *Geochemistry International* **50**, 1-7.
- Navrotsky A. (2011). Nanoscale effects on thermodynamics and phase equilibria in oxide systems. *ChemPhysChem* **12**, 2207 – 2215.
- Nielsen L.C., De Yoreo J.J., and DePaolo D.J. (2013). General model for calcite growth kinetics in the presence of impurity ions. *Geochimica et Cosmochimica Acta* **115**, 100-114.

- Palandri J. and Kharaka Y. (2004). A compilation of rate parameters of water-mineral interaction kinetics for application to geochemical modelling. U.S.G.S. Open File Report 2004-1068, Menlo Park CA, 70 p.
- Parkhurst D.L. and Appelo C.A.J. (1999). User's guide to PHREEQC (Version 2): U.S.G.S. WRIR 99-4259, 312 p.
- Parkhurst D.L., Kipp K.L., and Charlton S.R. (2010). PHAST Version 2. U.S.G.S. Techn. Methods 6–A35, 235 p.
- Schott J., Oelkers E.H., Bénézeth P. Goddériss, Y., and François, L. (2012). Can accurate kinetic laws be created to describe chemical weathering? *Comptes Rendus Geoscience* **344**, 568-585.
- Schott J., Pokrovsky O. S., and Oelkers E. H. (2009). The link between mineral dissolution/ precipitation kinetics and solution chemistry. Chapter 6 in *RiMG* **70**, 207-258.
- Scislewski A. and Zuddas P. (2010). Estimation of reactive mineral surface area during water-rock interaction using fluid chemical data. *Geochimica et Cosmochimica Acta* **74**, 6996–7007.
- Shao H., Dmytrieva S.V., Kolditz O., Kulik D.A., Pfingsten W., and Kosakowski G. (2009). Modeling reactive transport in non-ideal aqueous–solid solution system. *Applied Geochemistry* **24**, 1287-1300.
- Tadros M.E., Skalny J., and Kalyoncu, R.S. (1976). Kinetics of calcium hydroxide crystal growth from solution. *J. Colloid Interface Science* **55**, 20-24.
- Teng H.H., Dove P.M., and De Yoreo, J.J. (2000). Kinetics of calcite growth: Surface processes and relationships to macroscopic rate laws. *Geochimica et Cosmochimica Acta* **64**, 2255-2266.
- Tesoriero A. J. and Pankow J. F. (1996). Solid solution partitioning of Sr^{2+} , Ba^{2+} , and Cd^{2+} to calcite. *Geochimica et Cosmochimica Acta* **60**, 1053-1063.
- Thien B.M.J., Kulik D.A., and Curti E. (2014). A unified approach to model uptake kinetics of trace elements in complex aqueous – solid solution systems. *Applied Geochemistry* **41**, 135-150.
- Thien B.M.J., Kulik D.A., and Curti E. (2013). Modeling trace element uptake kinetics in secondary minerals. *Procedia Earth and Planetary Science* **7**, 838-841.
- Thoenen T. (2012). The PSI/Nagra Chemical Thermodynamic Database 12/07: Compilation of updated and new data with respect to the Nagra/PSI Chemical Thermodynamic Data Base 01/01. PSI Internal Report TM-44-12-06, Paul Scherrer Institut, Villigen, Switzerland.
- Tomazic B., Mohanty R., Tadros M, and Estrin J. (1986). Crystallization of calcium hydroxide from aqueous solution. II. Observations of growth, morphology and secondary nucleation. *Journal of Crystal Growth* **75**, 339-347.
- Wadell H. (1935). Volume, shape and roundness of quartz particles. *Journal of Geology* **43**, 250–280.
- Wagner T., Kulik D.A., Hingerl F.F., and Dmytrieva S.V. (2012). GEM-Selektor geochemical modeling package: TSolMod C++ class library and data interface for multicomponent phase models. *Canadian Mineralogist* **50**, 1173-1195.
- Watson, E. B. (2004). A conceptual model for near-surface kinetic controls on the trace-element and stable isotope composition of abiogenic calcite crystals. *Geochimica et Cosmochimica Acta* **68**, 1473-1488.
- Wolthers M., Nehrke G., Gustafsson J. P., and Van Cappellen P. (2012). Calcite growth kinetics: Modeling the effect of solution stoichiometry. *Geochimica et Cosmochimica Acta* **77**, 121-134.
- Wu W. and Nancollas G.H. (1999). Determination of interfacial tension from crystallization and dissolution data: a comparison with other methods. *Advances in Colloid and Interface Science* **79**, 229-279.

Appendix 1: Data structure for the kinetic rate law parameters transfer in the TKinMet class.

As follows from the above theoretical background (Sections 1 to 3): for k-th phase (Phase definition), the following flags should be used:

kin_t[2] Type of mineral-aqueous/gas reaction kinetic rate model (KinProCode)

Code	Comment	
N	not defined	
M	Kinetics of generic dissolution/precipitation (no uptake, ionex, adsorption)	
U	Kinetics of uptake/entrapment (of minor/trace element) into solid solution	In work
X	Kinetics of ion exchange (clays, C-S-H, zeolites, ...)	TBD
A	Kinetics of adsorption (on MWI), redox	TBD
P	Advanced kinetics of nucleation and precipitation (with PSD)	

kin_t[3] Code of the particular form of kinetic model (KinModCode)

Code	Comment	
N	not defined	
T	Generic TST model following (Shott ea 2012) with Hellevang nucleation rate	In work
P	Dissolution model of the form (Palandri 2004)	In work
W	Carbonate growth model following (Wolthers 2012)	TBD
U	Mineral nucleation and growth model with nuclei/particle size distribution	

kin_t[4] Type of the uptake kinetics model (KinSorpCode)

Code	Comment	
N	not defined	
E	Unified entrapment model (Thien,Kulik,Curti 2014)	TBD
M	DePaolo (2011) uptake kinetics model	TBD
G	Growth (surface) entrapment model (Watson 2004)	In work
F	Fast ion exchange kinetics (e.g. montmorillonite, CSH)	TBD
L	Slow ion exchange kinetics (e.g. illite, zeolites)	TBD
I	Adsorption inhibition	TBD
P	Solid solution nucleation model (Prieto 2013)	TBD

kin_t[5] Type of metastability links of this phase to other phases (KinLinkCode)

Code	Comment	
N	not defined	
S	link to (fraction of) solid substrate surface	TBD
P	link to (fraction of) solid substrate (pore) volume	TBD
M	link to (fraction of) solid substrate mass	

kin_t[6] Type of particle/pore size distribution and SSA correction (KinSizedCode)

Code	Comment	
N	not defined	
U	Uniform particle/pore size distribution	TBD
B	Binodal particle/pore size distribution	TBD
F	Empirical distribution function	

`kin_t[7]` Reserved code of kinetic rate model (KinResCode)

Code	Comment	
N	not defined	
A	surface-scaled rate model (k in mol/m ² /s)	
V	pore-volume-scaled model (k in mol/m ³ /s)	TBD

Dimensions of arrays of kinetic rate parameters

Label	Symbol	Description	Default
nPRk	$n(r)_k$	number of ‘parallel reactions’ that affect amount constraints for k -th phase (1, 2, 3, ...), at least one for dissolution, one for precipitation, optionally one for nucleation	2
nSkr	$n(j)_{k,r}$	total number of (aqueous or gaseous or surface) species from other reacting phases involved (assuming that in each ‘parallel reaction’, the same list of external reacting species is used)	0
nrpC		number of parameter coefficients involved in “parallel reaction” terms	0 or 14
naptC		number of parameter coefficients ($b_{j,k,r}$) per species involved in ‘activity product’ terms	1
numpC		number of the uptake model parameter coefficients (per end member)	0 or 8

Kinetic rate parameters arrays:

<code>fesAr</code>	$\theta_{k,r}$	effective fractions of surface area of solid related to different parallel reactions [nPRk]	1
<code>Ascp</code>	up to nAscC A_S shape/size growth/dissolution correction parameters [nAscC]		

Index	Comment	
0	Ψ shape factor (dimensionless)	
1 Testino parameter	TBD
2		

`ocPRk[iPR][0]` operation codes for kinetic parallel reaction affinity terms [nPRk][2]

Code	Comment	
0	Classic TST term $(u_{k,r} + 1 - \Omega_k^{q_{k,r}})^{m_{k,r}}$	
1	Inverse TST term $(\Omega_k^{q_{k,r}} - 1 - u_{k,r})^{m_{k,r}}$	
2	Schott term $e^{-m_{k,r}/\Omega_k}$	
3	Hellmann term $1 - e^{-(q_{k,r} \ln \Omega_k)^{m_{k,r}}}$	
4	Teng term $m_{k,r} (\Omega_k - 1) \cdot \ln \Omega_k$	
5	Teng nucleation term $\Omega_k^{m_{k,r}}$	
6	Fritz nucleation term $(\Omega_k - \Omega_{k,eff})^{m_{k,r}}$	TBD
7	Helevang nucleation rate term $k_N \exp \left\{ -\Gamma_k \left(\frac{1}{T^{3/2} \ln \Omega} \right)^2 \right\}$	In work

ocPRk[iPR][1]	index of surface patch (crystal particle face) [nPRk], max 3	0
---------------	--	---

rpCon table of kinetic rate constants for “parallel reaction” regions [nPRk][nrpC]

Parameter coefficients for each parallel reaction (to enter into an iPR row):

Index	Comment	Default
0	Standard-temperature net rate constant $\kappa_{k,r}^+$ or $\kappa_{k,r}^-$ (mol/m ² /s)*	0
1	Standard-temperature gross rate constant $K_{k,r}^+$ or $K_{k,r}^-$ (mol/m ² /s)**	0
2	Arrhenius factor $\Lambda_{k,r}$	1
3	Activation energy $E_{k,r}$ (J mol ⁻¹),	0
4	$b_{I,k,r}$: empirical power parameter related to ionic strength I	0
5	$b_{pH,k,r}$: empirical power parameter related to pH	0
6	$b_{pe,k,r}$: empirical power parameter related to pe	0
7	$b_{Eh,k,r}$: empirical power parameter related to Eh, V	0
8	$p_{k,r}$: «reaction order» power parameter for the activity product term (in far-from-equilibrium case)	1
9	$q_{k,r}$: empirical power parameter in the affinity term	1
10	$m_{k,r}$: empirical power parameter for the affinity term	0
11	$u_{k,r}$: power parameter or constant in the affinity term	0 or 1
12	$\kappa_{N,k,r}^-$: Nucleation rate constant, mol/s/(dm ³ aq) (rpCon[r][0] to be set to -1)	1
13	$\Gamma_{N,k,r}$: Effective parameter of the Hellevang nucleation affinity term (K ³)	0

Notes. If the net rate constant is 0 and gross rate constant is not 0 then the gross rate constant will be used, and vice versa. If both are not 0 then the net rate constant will be used; if both are 0 then this parallel reaction is disabled. The *state of dissolution* of k-th phase is detected when $\Omega_k < 1 - \varepsilon_{kin}$; the *state of precipitation* – when $\Omega_k > 1 + \varepsilon_{kin}$; *equilibrium* – when $1 - \varepsilon_{kin} \leq \Omega_k \leq 1 + \varepsilon_{kin}$ ($10^{-8} \leq \varepsilon_{kin} \leq 10^{-3}$ is the numerical tolerance for kinetic calculations). If the net rate constant is positive ($\kappa_{k,r}^+$) and the state is *dissolution* then this parallel reaction will be used, but if the state is precipitation then this parallel reaction will be skipped. If the net rate constant is negative ($\kappa_{k,r}^-$) and the state is *precipitation* then this reaction will be used with $|\kappa_{k,r}^-|$, but if the state is *dissolution* then this reaction will be skipped. In a single mineral phase definition, via multiple “parallel reactions”, these rules allow setup of both dissolution and precipitation kinetics, according to different mechanisms, and/or applicable to several aqueous composition regions at varying temperatures.

apCon array of parameters per species in “activity product” terms [nPRk][nSKr][napC]

[0] $b_{j,k,r}$: (reaction stoichiometry coefficient) parameter (default 0, disables the j-th species contribution to the activity product).

1DCr common list of record keys (from the project system) of DComp, ReacDC records of species involved in the activity product terms [nSKr] (in MULTI, converted to a composite vector of indexes of dependent components xSKr involved in parallel reactions activity product terms)

Uptake kinetics models

umpCon Array of uptake model parameters [nDC][numpC]

Uptake model parameters

Index	Comment	Symbol	Default
0	Surface enrichment/depletion factor	F_{Tr}	1
1	Tr fractionation coefficient in solid solution in equilibrium with the medium	$\Delta_{Tr,Hc,eq} = \alpha_{eq}$	1
2	Tr surface diffusivity nm ² /s	D_s	0
3	lattice diffusion coefficient nm ² /s	D_l	0
4	half-thickness of surface enriched/depleted layer (nm)	l	0
5	multiplier linking l to the maximal thickness of the diffusivity region	m	1